SCIENCE CHINA
Chemistry

•ARTICLES•
SPECIAL TOPIC: Photovoltaics

July 2019 Vol.62 No.7: 829–836
https://doi.org/10.1007/s11426-018-9429-1

High open-circuit voltage organic solar cells enabled by a difluorobenzoxadiazole-based conjugated polymer donor

Ruiwen Zhang†, Junyi Wang†, Xi Liu†, Shuting Pang, Chunhui Duan*, Fei Huang* & Yong Cao

Institute of Polymer Optoelectronic Materials and Devices, State Key Laboratory of Luminescent Materials and Devices, South China University of Technology, Guangzhou 510640, China

Received December 18, 2018; accepted January 23, 2019; published online March 12, 2019

A new polymer donor based on 3,3′-difluoro-2,2′-bithiophene (2F2T) and difluorobenzoxadiazole (ffBX), named 2F2T-ffBX, is designed and synthesized. The organic solar cell (OSC) based on 2F2T-ffBX donor and [6,6]-phenyl-C60-butyl acid methyl ester ([60]PCBM) acceptor exhibits a high efficiency of 7.3% with a high open-circuit voltage (V_{oc}) of 1.03 V. When blended with perylenediimide-based acceptor (PDI6), the corresponding OSC shows a higher V_{oc} of 1.19 V with a low energy loss of 0.50 eV but a much lower efficiency of 2.0%. The detailed analyses including charge generation, transport, recombination properties, and morphology were performed to understand the performance of corresponding devices.

organic solar cells, conjugated polymer, difluorobenzoxadiazole, open-circuit voltage, energy loss

Citation: Zhang R, Wang J, Liu X, Pang S, Duan C, Huang F, Cao Y. High open-circuit voltage organic solar cells enabled by a difluorobenzoxadiazole-based conjugated polymer donor. *Sci China Chem*, 2019, 62: 829–836, https://doi.org/10.1007/s11426-018-9429-1

1 Introduction

In the past decade, organic solar cells (OSCs) have gained enormous attention due to the unique advantages of light weight, flexibility, and low-cost processing [1–6]. Recently, significant progress has been made in improving the performance of OSCs, with power conversion efficiency (PCE) over 14% for single junction devices and over 17% for tandem solar cells being achieved [7–10]. However, significant effort is still needed to transfer lab-scale OSCs to industrial application [11]. One of the key reasons that limit PCEs of OSCs is the modest open-circuit voltage (V_{oc}) attributed to the large energy loss (E_{loss}) from the optical bandgap (E_g) of the active layer material to the V_{oc} of OSCs [12–14]. The E_{loss} in OSCs is analytically defined as $E_{loss}=E_g-qV_{oc}$, where E_g is the lowest optical bandgap among donor and acceptor materials, q is elementary charge [12]. High performance inorganic/hybrid solar cells such as crystalline silicon and perovskite solar cells show E_{loss} values in the range of 0.30–0.55 eV [13]. However, the E_{loss} of most state-of-the-art OSCs is in the range of 0.7–1.0 eV, although a few systems show E_{loss} below 0.7 eV [12–29]. As a result, it is hardly to offer V_{oc} over 1.0 V for fullerene based OSCs at PCE>10%, and only a few non-fullerene based OSCs obtained V_{oc} over 1.1 V at PCE>6% [30,31]. A few promising polymer donors with suitable energy levels to realize low E_{loss} have been reported based on building blocks such as diketopyrrolopyrrole (DPP), pyridyl[2,1,3]thiadiazole (PT), [1,2,5]thiadiazolo[3,4-f]isoindole-5,7-dione (TID), difluorobenzotriazole (FTAZ), difluorobenzoxadiazole (ffBX), and difluorobenzothiadiazole (ffBT), which offered E_{loss} lower than 0.6 eV when blended with fullerene or non-fullerene acceptors [15,16,18,19,32–34].

Previously, our group has reported a polymer donor based on 5,6-difluoro-2,1,3-benzoxadiazole (ffBX) and benzo[1,2-*b*:4,5-*b*′]dithiophene (BDT) with 2-decyltetradecyl (DT) side chain, named BDT-ffBX-DT, which exhibits a PCE of 9.4%

†These authors contributed equally to this work.
*Corresponding authors (email: duanchunhui@scut.edu.cn; msfhuang@scut.edu.cn)

when blended with [6,6]-phenyl-C60-butyl acid methyl ester ([60]PCBM) [35]. However, the E_{loss} of BDT-ffBX-DT:[60]PCBM-based OSC is 0.8 eV, although this fullerene-based device shows a V_{oc} of 0.93 V [35]. Afterwards, we reported the OSCs by blending BDT-ffBX-DT with perylenediimide-based acceptors (SFPDI, PDI4, and PDI6) instead of [60]PCBM acceptor. A high PCE of 7.5% associated with a very high V_{oc} (>1.10 V) and low E_{loss} (<0.60 V) was obtained for the BDT-ffBX-DT:PDI4 device [31]. More importantly, the BDT-ffBX-DT:SFPDI device shows a high V_{oc} up to 1.23 V, which is among the highest values reported for OSCs with a PCE beyond 6%, corresponding to a very low E_{loss} of 0.48 eV and an extremely low non-radiative recombination loss of 0.20 V [29,31]. These results indicate that ffBX is a useful building block for the synthesis of conjugated polymer donors to realize high performance and low E_{loss} OSCs.

3,3′-Difluoro-2,2′-bithiophene (2F2T) is one of the famous building blocks for constructing conjugated donor-acceptor (D-A) polymers in previous reports owing to the unique merits such as moderate electron-donating ability, suitable energy level, and coplanar structure [36–41]. However, most of these 2F2T based conjugated polymers show moderate V_{oc} (0.80–0.95 V) and high E_{loss} (~0.70 eV) in fullerene based OSCs or non-fullerene based OSCs [36–41]. It is well known that V_{oc} is proportional to the energy level difference between the lowest unoccupied molecular orbital (LUMO) of the acceptor and the highest occupied molecular orbital (HOMO) of the donor [42]. It means that the lower HOMO level of polymer donor could benefit V_{oc} and E_{loss} of the corresponding OSCs. We thus focus on lowering HOMO energy level of 2F2T based conjugated polymer donors, aiming at enlarging energy level difference between the LUMO of the acceptor and the HOMO of the donor and enhancing V_{oc} and performance of the corresponding OSCs.

Herein, we report the design and synthesis of a new D-A conjugated polymer based on ffBX and 2F2T, which is named 2F2T-ffBX. The chemical structures of 2F2T-ffBX and the electron acceptors used in this study are shown in Figure 1. The four fluorine atoms in the repeat unit will not only downshift the energy levels but also improve the coplanarity of the polymer chain, which endow the corresponding polymer with suitable HOMO level and strong aggregation of the polymer chains. The OSC based on 2F2T-ffBX:[60]PCBM blend film exhibits a high efficiency of 7.3% with a V_{oc} of 1.03 V, which is among the highest levels with V_{oc}>1.0 V and PCE>6% for fullerene based OSCs (Figure 2(a)). When blended with non-fullerene acceptor (PDI6), the corresponding OSC shows a higher V_{oc} of 1.19 V with a low E_{loss} of 0.50 eV, which are both among the best results for PDI-based OSCs (Figure 2(c, d)). However, the 2F2T-ffBX:PDI6-based device shows much lower performance with a PCE of 2.0%. The detailed analyses of the OSCs based on the two different acceptors were investigated, including charge generation, transport, recombination properties, and morphology to understand the performance of corresponding devices.

2 Experimental

2.1 General details

The synthesis route of 2F2T-ffBX is described in Figure 3. [60]PCBM was purchased from Nano-C (USA). All of other chemicals were purchased from commercial supplies and used as received unless specifically stated. Molecular weight of the polymer was determined using an Agilent Technologies 220 high-temperature chromatograph (USA) in 1,2,4-trichlorobenzene at 150 °C using a calibration curve of polystyrene standards. UV-Vis spectra were recorded on a HP 8453 spectrophotometer (HP Development Company, USA). Square wave voltammetry (SWV) were measured on a CHI600D electrochemical workstation by using Bu_4NPF_6 (0.1 M) in acetonitrile as electrolyte and glassy-carbon, platinum, and saturated calomel electrode as the working, counter, and reference electrode, respectively. Potentials were referenced to the ferrocenium/ferrocene couple by using ferrocene as an internal standard.

2.2 Device fabrication and characterization

The OSCs devices based on 2F2T-ffBX and two different acceptors were fabricated with a device structure of indium tinoxide(ITO)/poly(3,4-ethylenedioxy-thiophene):poly(styrene sulfonate) (PEDOT:PSS)/active layer/poly[(9,9-bis(3-(*N*,*N*-dimethyl)-*N*-ethylammonium-propyl)-2,7-fluorene)-*alt*-2,7-(9,9-dioctylfluorene)]dibromide (PFN-Br)/Ag [43,44].

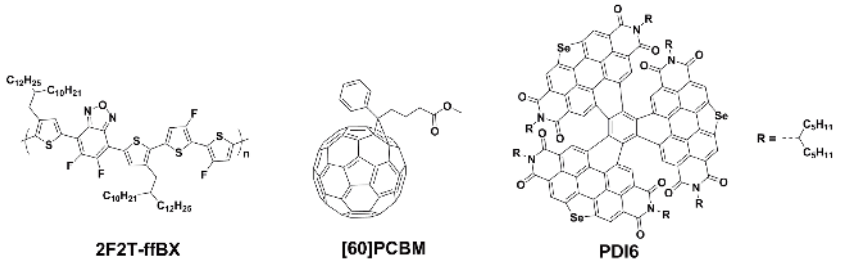

Figure 1 Chemical structures of 2F2T-ffBX, [60]PCBM, and PDI6.

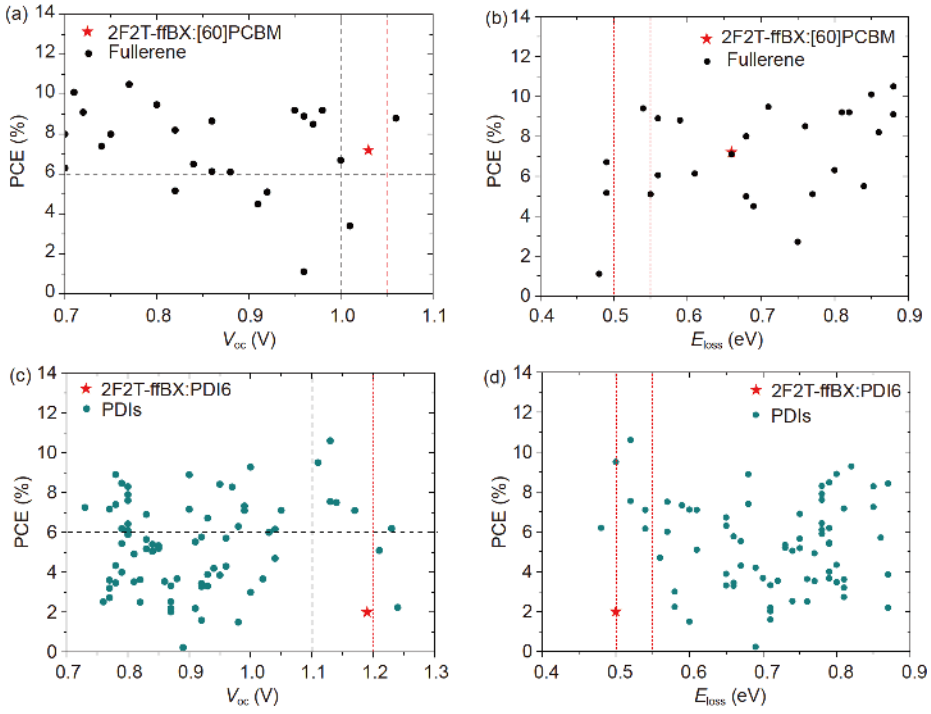

Figure 2 Plots of PCE versus (a, c) V_{oc} and (b, d) E_{loss} in various (a, b) fullerene-based and (c, d) PDI-based OSCs (color online).

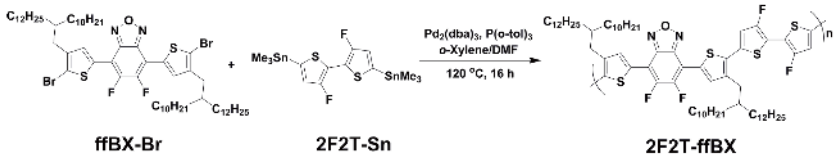

Figure 3 Synthesis route of the 2F2T-ffBX polymer.

The ITO glass substrates were cleaned sequentially under sonication with detergent water, deionized water, and isopropyl alcohol and then dried at 70 °C overnight, followed by a 4 min oxygen plasma treatment. Then a PEDOT:PSS layer (~40 nm) was spin-coated on top of ITO substrates and dried in air at 140 °C for 15 min. All substrates were then transferred to a glovebox under nitrogen (N_2) for the following fabrication of active layers. The weight ratio of donor:acceptor were kept at 1:1 and both 2F-2T:[60]PCBM and 2F-2T:PDI6 solutions were prepared in chlorobenzene with different additives. All solutions were kept on a hot plate at 95 °C for 6 h to ensure complete dissolution. Active layers were spin-coated from active layer solutions on the preheated substrates at 95 °C to obtain the required thicknesses (100–300 nm) by changing the concentration of the active layer solutions and the spinning speed. The active layer films were then vacuumed at a level of 1×10^{-7} Torr overnight to remove the residual additives. Then a PFN-Br buffer layer (~5 nm) was spin-coated from PFN-Br methanol solution at a concentration of 0.5 mg mL^{-1} on active layers and the samples were transferred to the vacuum chamber. At a vacuum level of 1×10^{-7} Torr, 90 nm of Ag was thermally deposited as the top electrode. The active area of all devices is 0.07 cm^2. The *J-V* curves were measured on a computer-controlled Keithley 2400 source meter (USA) under 1 sun illumination. The AM1.5G spectra came from a class solar simulator (Enlitech, Taiwan, China), and the light intensity was 100 mW cm^{-2} as calibrated by a China General Certification Center-certified reference monocrystal silicon cell (Enlitech, China). Before the *J-V* test, a physical mask with an aperture with precise area of 0.04 cm^2 was used to define the device area. The external quantum efficiency (EQE) spectra measurements were performed on a commercial EQE measurement system (QE-R3011, Enlitech, China).

3 Results and discussion

3.1 Synthesis

The synthesis of monomer 5,6-difluoro-4,7-bis(5-bromo-4-(2-decyltetradecyl)-2-thienyl)-2,1,3-benzoxadiazole (ffBX-Br) was shown in our previously work [35]. The monomer

(3,3′-difluoro-[2,2′-bithiophene]-5,5′-diyl)bis(trimethylstannane) (2F2T-Sn) was purchased from SunaTech Inc. (China). The synthesis route of 2F2T-ffBX is shown in Figure 3. To a degassed solution of ffBX-Br (0.15 mmol, 172.3 mg), 2F2T-Sn (0.15 mmol, 79.5 mg) in anhydrous chlorobenzene (1.5 mL), $Pd_2(dba)_3$ (2.1 mg, 0.00225 mmol) and tri(*o*-tolyl)phosphine (5.5 mg, 0.018 mmol) were added. Then the mixture was stirred at 120 °C for 12 h. The obtained gel was diluted with 3.5 mL anhydrous chlorobenzene, and then the mixture was stirred at 120 °C for additional 12 h, after which 2-(tributylstannyl) thiophene and 2-bromothiophene were sequentially added to the reaction with 2 h interval. After another 2 h, the reaction mixture was diluted with chlorobenzene, and refluxed with sodium *N*,*N*-diethylcarbamodithioate trihydrate (100 mg) for 2 h. After cooling to room temperature, the reaction mixture was precipitated in methanol and filtered through a Soxhlet thimble. The polymer was subjected to sequential Soxhlet extraction with acetone, hexane, dichloromethane, chloroform, and chlorobenzene under argon protection. The chlorobenzene fraction was concentrated under reduced pressure and precipitated in methanol to obtain the resulting polymer 2F2T-ffBX (170 mg, yield=90%). The number-average molecular weight (M_n) and polydispersity index (PDI) of 2F2T-ffBX were estimated by high-temperature gel permeation chromatography using 1,2,4-trichlorobenzene at 150 °C as an eluent calibrated with a series of monodispersed polystyrene standards. The M_n of 2F2T-ffBX is 50.1 kDa, and with a PDI of 1.6.

3.2 Optical properties

Figure 4(a) illustrates the normalized absorption spectra of the 2F2T-ffBX in chlorobenzene (CB) solution and thin film state. Both in solution and thin film state, the high-energy absorption bands of 2F2T-ffBX at about 425 nm are attributed to localized electronic transitions of the aromatic rings, while the border low-energy absorption bands at about 690 nm arises from π-π* transitions with intramolecular charge transfer (ICT) character between the electron-rich and electron-deficient moieties. The polymer film shows the same absorption onset as the polymer solution in chlorobenzene, corresponding an optical bandgap of E_g=1.69 eV. In Figure S1 (Supporting Information online), we presented the absorption spectra of 2F2T-ffBX in chlorobenzene solutions at different temperatures. The three peaks of the curves keep at the same wavelength under different temperatures. These results suggest that the polymer shows strong aggregation of the main chain packing, which benefits the hole transport property in the donor domain of the corresponding blend film.

3.3 Electrochemical properties

To estimate the energy levels of 2F2T-ffBX, [60]PCBM, and PDI6, the electrochemical properties were investigated by square wave voltammetry (SWV), which are shown in Figure S2. As shown in Figure 4(d), the HOMO and LUMO of 2F2T-ffBX are calculated to be −5.37 and −3.49 eV, respectively. The deep-lying HOMO level is beneficial to obtaining high V_{oc} in OSCs. For [60]PCBM, the HOMO and LUMO levels are −6.10 and −3.96 eV. Hence, the HOMO-HOMO offset (ΔHOMO) and LUMO-LUMO offset (ΔLUMO) between 2F2T-ffBX and [60]PCBM is 0.73 and 0.47 eV, which could provide enough driving forces to realized efficient exciton dissociation and charge separation [42]. Meanwhile, the HOMO and LUMO levels of PDI6 are −6.01 and −3.76 eV, respectively, the up-lying LUMO level of PDI6 will benefit to the final V_{oc} and E_{loss} of the corresponding OSCs as compared to [60]PCBM.

3.4 Photovoltaic performance

The photovoltaic parameters are summarized in Table 1, and the corresponding *J*-*V* curves are shown in Figure 5(a). Device optimization of donor:acceptor weight ratio, solvent,

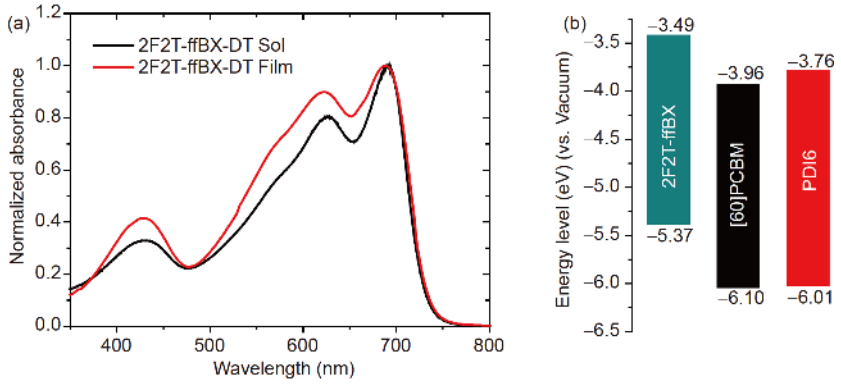

Figure 4 (a) Normalized absorption spectra of 2F2T-ffBX in chlorobenzene solution and as thin film; (b) energy level alignments of 2F2T-ffBX, [60]PCBM and PDI6 (color online).

Table 1 Performance parameters of the 2F2T-ffBX:[60]PCBM and 2F2T-ffBX:PDI6 solar cells under AM1.5G illumination (100 mW cm^{-2})

Acceptor	V_{oc} (V)	J_{sc} (mA cm^{-2})	FF	PCE (%)	PCE (ave) (%)	E_{loss} (eV)
[60]PCBM	1.03	10.3	0.69	7.3	7.0	0.66
PDI6	1.19	5.0	0.33	2.0	1.8	0.50

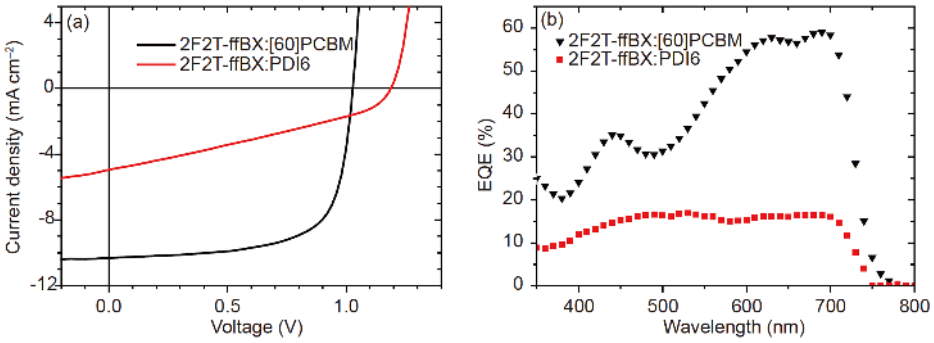

Figure 5 (a) *J-V* curves and (b) EQE spectra of 2F2T-ffBX:[60]PCBM and 2F2T-ffBX:PDI6 devices under the illumination of an AM1.5G solar simulator, 100 mW cm^{-2} (color online).

solvent additive, annealing temperature of spin coating, thermal annealing, fullerene acceptors, active layer thickness, and device structure were summarized in Tables S1–S5 (Supporting Information online). The 2F2T-ffBX:[60]PCBM-based device exhibited an excellent V_{oc} of 1.03 V, along with a E_{loss} of 0.66 eV. The V_{oc} of the device ranks the outstanding level reported in the literature for fullerene-based OSCs. It is worth noting that high fill factor (FF) of 0.69 can be obtained, suggesting efficient charge generation and collection in the device. Combining with a short-circuit current density (J_{sc}) of 10.3 mA cm^{-2}, a PCE of 7.3% can be realized by the 2F2T-ffBX:[60]PCBM-based device at the optimized active layer thickness of 110 nm. Further increasing the thickness of active layer to 250 nm, the 2F2T-ffBX:[60]PCBM blend still offers a PCE of 7.0% with V_{oc} of 0.99 V and FF of 0.58 (Table S3 and Figure S4). As known to all, thick active layer is a very critical prerequisite to support large-area fabrication of OSCs. Combining with the use of low-cost acceptor [60]PCBM, 2F2T-ffBX shows a potential for low-cost, large-area fabrication of OSCs. In terms of 2F2T-ffBX:PDI6-based device, a high V_{oc} of 1.19 V and a low E_{loss} of 0.50 eV can be achieved, which are among the best results for the PDI-based OSCs reported up to date. However, the 2F2T-ffBX:PDI6-based device suffered from low J_{sc} and FF, leading to a low PCE of 2.0%. The absorption spectra of the blend films shown in Figure S2 evidence the efficient light-harvesting of the 2F2T-ffBX:PDI6, suggesting that the low J_{sc} is caused by other factors. To understand the performance difference of the solar cells based on two different acceptors further investigations were performed, which will be discussion in more details in the following parts.

The vastly different J_{sc} values of both OSCs can be confirmed by the EQE spectra of the devices, as shown in Figure 3(b). The 2F2T-ffBX:[60]PCBM-based device shows high EQE response over 60% from 620 to 700 nm, indicating the efficient charge generation, transport, and collection in the device. However, the 2F2T-ffBX:PDI6-based device shows poor EQE response (<15%) in a wide spectral range, which is consistent with the low J_{sc} and FF of the devices.

3.5 Charge generation, transport, and recombination

To further investigate the performance difference between the OSCs of 2F2T-ffBX:[60]PCBM and 2F2T-ffBX:PDI6, the EQE spectra under different voltage bias were recorded. As shown in Figure 6, the EQE curves of the two kinds of devices show distinctly different trends under voltage bias. When the voltage bias on the 2F2T-ffBX:[60]PCBM device was changed from 0 to −2.0 V, the EQE spectra are almost unchanged, suggesting the efficient charge generation in these devices. However, the EQE spectra of the 2F2T-ffBX:PDI6 devices under different voltage bias shows obvious changes. A gradually increase of EQE response can be observed when a higher voltage bias was applied to the device. Specifically, the EQE response is doubled when −2 V voltage bias was applied as compared to the unbiased device. These results indicate that 2F2T-ffBX:PDI6 device suffers from inefficient charge generation under short-circuit condition, which is a part of reasons for the low PCE, while the devices can generate charges more efficiently with the help of electrical field.

Moreover, space-charge-limited-current (SCLC) method was employed to measure the hole mobility and electron mobility of both 2F2T-ffBX:[60]PCBM blend and 2F2T-ffBX:PDI6 blend (Figure 7(a, b)). The 2F2T-ffBX:[60]

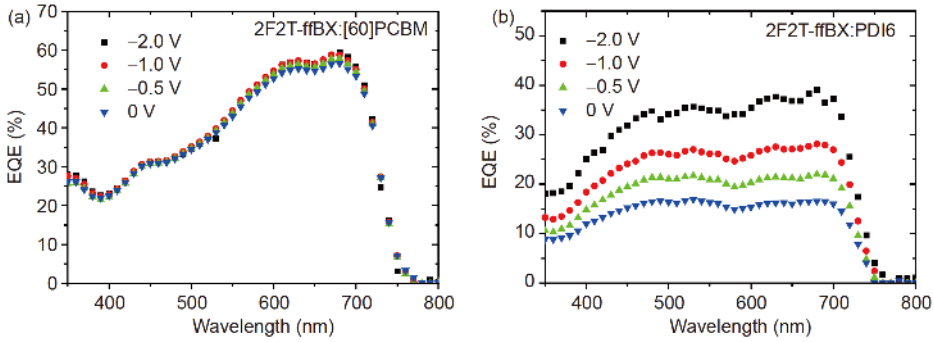

Figure 6 EQE spectra under different voltage bias of (a) 2F2T-ffBX:[60]PCBM and (b) 2F2T-ffBX:PDI6 devices (color online).

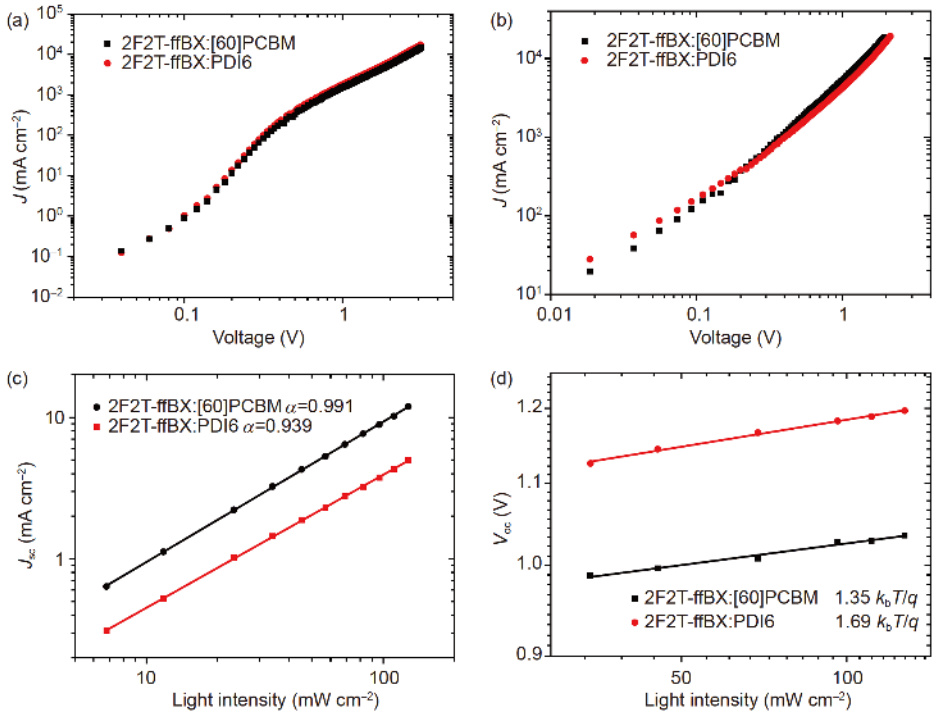

Figure 7 Current intensity versus voltage characteristics of (a) hole-only and (b) electron-only devices based on 2F2T-ffBX:[60]PCBM and 2F2T-ffBX:PDI6 blends; (c) J_{sc} and (d) V_{oc} of the devices based on 2F2T-ffBX:[60]PCBM and 2F2T-ffBX:PDI6 as a function of light intensity (color online).

PCBM blend exhibits hole/electron mobilities of 2.1/1.0×10^{-3} cm^2 V^{-1} s^{-1} while the 2F2T-ffBX:PDI6 blend shows hole/electron mobilities of 2.6/2.4×10^{-3} cm^2 V^{-1} s^{-1}, suggesting the charge transport of the devices are comparable and balanced. The J_{sc} and V_{oc} at various light intensities were acquired to investigate the charge recombination characteristics of the devices. The results are plotted in Figure 7(c, d). It is well known that the relationship between J_{sc} and P_{light} can be described as $J_{sc} \propto (P_{light})^{\alpha}$, where P_{light} is the light intensity and α is the power-law component that will be equal to 1.0 if there is no bimolecular recombination of the charge carriers [45]. For 2F2T-ffBX:[60]PCBM-based device, an α value of 0.991 was recorded, suggesting there is only a negligible bimolecular recombination inside the device. For the 2F2T-ffBX:PDI6 device, a lower α value of 0.939 was measured, which implies this device suffered from more serious bimolecular recombination. The relationship between V_{oc} and light intensity can reveal the degree of trap-assisted recombination in the devices. The slope of V_{oc} versus ln$P$ will be k_BT/q when trap-assisted recombination is negligible, while the slope will be close to 2.0 k_BT/q if trap-assisted recombination is the dominant recombination mechanism (where q, T and k_B are the elementary charge, temperature in Kelvin, and Boltzmann constant) [45]. The results reveal 2F2T-ffBX:PDI6-based device shows more severe trap-assisted recombination as evidenced by its higher slope value of 1.69 k_BT/q as compared to 1.35 k_BT/q of 2F2T-ffBX:[60]PCBM-based device. The recombination analyses thus explained the difference in device performance of the OSCs based on 2F2T-ffBX:[60]PCBM and 2F2T-ffBX:PDI6.

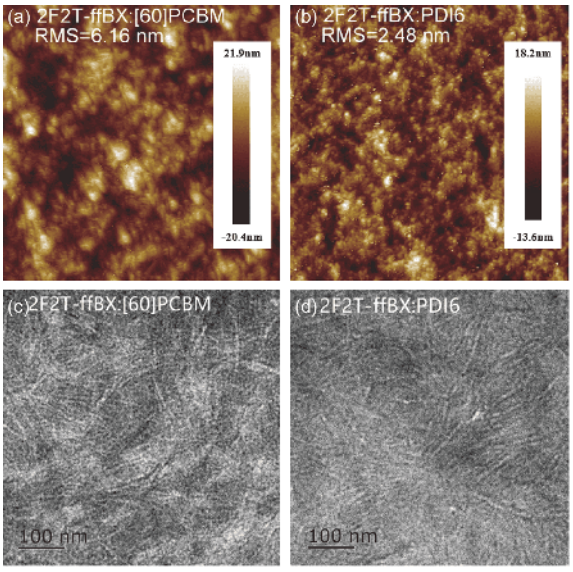

Figure 8 The (a, b) AFM and (c, d) TEM images of (a, c) 2F2T-ffBX:[60]PCBM film and (b, d) 2F2T-ffBX:PDI6 film (color online).

3.6 Morphology

The surface and bulk morphologies of the active layers were studied by atomic force microscopy (AFM) and transmission electron microscopy (TEM). The images are illustrated in Figure 8. As shown in AFM images (Figure 8(a, b), 2F2T-ffBX:[60]PCBM film exhibits a root-mean-square (RMS) roughness of 6.16 nm, while the 2F2T-ffBX:PDI6 film shows a RMS roughness of 2.48 nm, suggesting that the former is more phased separated than the latter. Generally, a less phase separated blend morphology is beneficial to exciton diffusion to donor:acceptor interface and can provide large interface area for exciton dissociation, the poorer device performance of 2F2T-ffBX:PDI6 should be ascribed to the unfavorable energy level alignment rather than blend morphology. In the TEM images (Figure 8(c, d)), fibers can be observed for both the 2F2T-ffBX:[60]PCBM film and 2F2T-ffBX:PDI6 film, providing continuous channels for efficient charge transport, which is consistent with the hole/electron mobilities measured from single carrier devices.

4 Conclusions

In summary, a new conjugated polymer 2F2T-ffBX based on ffBX and 2F2T was designed and synthesized. The four fluorine atoms in the repeat unit will not only downshift the energy levels but also improve the coplanarity of the polymer chain, which contribute the corresponding polymer suitable HOMO level and strong aggregation of the polymer chains. The solar cell based on 2F2T-ffBX:[60]PCBM blend film exhibits a high efficiency of 7.3% with a V_{oc} of 1.03 V. When blended with a non-fullerene acceptor (PDI6), the corresponding OSC shows a higher V_{oc} of 1.19 V with a low E_{loss} of 0.50 eV but a much lower PCE of 2.0%. The detailed analyses including charge generation, transport, recombination, and morphology were performed to understand the performance of the solar cells. The results suggest that the development of new conjugated polymers for achieving high V_{oc} and low E_{loss} in organic solar cells should consider the energy levels, aggregation properties, and transport abilities simultaneously.

Acknowledgements This work was supported by the Ministry of Science and Technology (2017YFA0206600, 2014CB643501), the National Natural Science Foundation of China (21875072, 21520102006, 91633301), and the Recruitment Program of Global Youth Experts of China.

Conflict of interest The authors declare that they have no conflict of interest.

Supporting information The supporting information is available online at http://chem.scichina.com and http://link.springer.com/journal/11426. The supporting materials are published as submitted, without typesetting or editing. The responsibility for scientific accuracy and content remains entirely with the authors.

1 Yu G, Gao J, Hummelen JC, Wudl F, Heeger AJ. *Science*, 1995, 270: 1789–1791
2 Brabec CJ, Gowrisanker S, Halls JJM, Laird D, Jia S, Williams SP. *Adv Mater*, 2010, 22: 3839–3856
3 Li Y. *Acc Chem Res*, 2012, 45: 723–733
4 Lu L, Zheng T, Wu Q, Schneider AM, Zhao D, Yu L. *Chem Rev*, 2015, 115: 12666–12731
5 Krebs FC, Fyenbo J, Jørgensen M. *J Mater Chem*, 2010, 20: 8994
6 Zhang G, Zhao J, Chow PCY, Jiang K, Zhang J, Zhu Z, Zhang J, Huang F, Yan H. *Chem Rev*, 2018, 118: 3447–3507
7 Li H, Xiao Z, Ding L, Wang J. *Sci Bull*, 2018, 63: 340–342
8 Zhang S, Qin Y, Zhu J, Hou J. *Adv Mater*, 2018, 30: 1800868
9 Li S, Ye L, Zhao W, Yan H, Yang B, Liu D, Li W, Ade H, Hou J. *J Am Chem Soc*, 2018, 140: 7159–7167
10 Meng L, Zhang Y, Wan X, Li C, Zhang X, Wang Y, Ke X, Xiao Z, Ding L, Xia R, Yip HL, Cao Y, Chen Y. *Science*, 2018, 361: 1094–1098
11 https://www.nrel.gov/pv/assets/images/efficiency-chart.png, accessed on 2018-11-29
12 Veldman D, Meskers SCJ, Janssen RAJ. *Adv Funct Mater*, 2009, 19: 1939–1948
13 Yao J, Kirchartz T, Vezie MS, Faist MA, Gong W, He Z, Wu H, Troughton J, Watson T, Bryant D, Nelson J. *Phys Rev Appl*, 2015, 4: 014020
14 Nayak PK, Cahen D. *Adv Mater*, 2014, 26: 1622–1628
15 Wang M, Wang H, Yokoyama T, Liu X, Huang Y, Zhang Y, Nguyen TQ, Aramaki S, Bazan GC. *J Am Chem Soc*, 2014, 136: 12576–12579
16 Li W, Hendriks KH, Furlan A, Wienk MM, Janssen RAJ. *J Am Chem Soc*, 2015, 137: 2231–2234
17 Gao K, Li L, Lai T, Xiao L, Huang Y, Huang F, Peng J, Cao Y, Liu F, Russell TP, Janssen RAJ, Peng X. *J Am Chem Soc*, 2015, 137: 7282–7285
18 Wang C, Xu X, Zhang W, Bergqvist J, Xia Y, Meng X, Bini K, Ma W, Yartsev A, Vandewal K, Andersson MR, Inganäs O, Fahlman M, Wang E. *Adv Energy Mater*, 2016, 6: 1600148
19 Lin H, Chen S, Li Z, Lai JYL, Yang G, McAfee T, Jiang K, Li Y, Liu Y, Hu H, Zhao J, Ma W, Ade H, Yan H. *Adv Mater*, 2015, 27: 7299–7304
20 Yao H, Chen Y, Qin Y, Yu R, Cui Y, Yang B, Li S, Zhang K, Hou J. *Adv Mater*, 2016, 28: 8283–8287

21 Chen S, Liu Y, Zhang L, Chow PCY, Wang Z, Zhang G, Ma W, Yan H. *J Am Chem Soc*, 2017, 139: 6298–6301
22 Xiao Z, Jia X, Li D, Wang S, Geng X, Liu F, Chen J, Yang S, Russell TP, Ding L. *Sci Bull*, 2017, 62: 1494–1496
23 Cheng P, Zhang M, Lau TK, Wu Y, Jia B, Wang J, Yan C, Qin M, Lu X, Zhan X. *Adv Mater*, 2017, 29: 1605216
24 Yao Z, Liao X, Gao K, Lin F, Xu X, Shi X, Zuo L, Liu F, Chen Y, Jen AKY. *J Am Chem Soc*, 2018, 140: 2054–2057
25 Xu X, Yu T, Bi Z, Ma W, Li Y, Peng Q. *Adv Mater*, 2018, 30: 1703973
26 Yuan J, Qiu L, Zhang ZG, Li Y, Chen Y, Zou Y. *Nano Energy*, 2016, 30: 312–320
27 Wang T, Feng L, Yuan J, Jiang L, Deng W, Zhang ZG, Li Y, Zou Y. *Sci China Chem*, 2018, 61: 206–214
28 Zhang Y, Yao H, Zhang S, Qin Y, Zhang J, Yang L, Li W, Wei Z, Gao F, Hou J. *Sci China Chem*, 2018, 61: 1328–1337
29 Zhang Y, Guo X, Guo B, Su W, Zhang M, Li Y. *Adv Funct Mater*, 2017, 27: 1603892
30 Baran D, Kirchartz T, Wheeler S, Dimitrov S, Abdelsamie M, Gorman J, Ashraf RS, Holliday S, Wadsworth A, Gasparini N, Kaienburg P, Yan H, Amassian A, Brabec CJ, Durrant JR, McCulloch I. *Energy Environ Sci*, 2016, 9: 3783–3793
31 Liu X, Du X, Wang J, Duan C, Tang X, Heumueller T, Liu G, Li Y, Wang Z, Wang J, Liu F, Li N, Brabec CJ, Huang F, Cao Y. *Adv Energy Mater*, 2018, 8: 1801699
32 Zhao J, Li Y, Hunt A, Zhang J, Yao H, Li Z, Zhang J, Huang F, Ade H, Yan H. *Adv Mater*, 2016, 28: 1868–1873
33 Lin H, Chen S, Hu H, Zhang L, Ma T, Lai JYL, Li Z, Qin A, Huang X, Tang B, Yan H. *Adv Mater*, 2016, 28: 8546–8551
34 Liu J, Chen S, Qian D, Gautam B, Yang G, Zhao J, Bergqvist J, Zhang F, Ma W, Ade H, Inganäs O, Gundogdu K, Gao F, Yan H. *Nat Energy*, 2016, 1: 16089
35 Wang J, Wang S, Duan C, Colberts FJM, Mai J, Liu X, Jia X, Lu X, Janssen RAJ, Huang F, Cao Y. *Adv Energy Mater*, 2017, 7: 1702033
36 Liu Y, Zhao J, Li Z, Mu C, Ma W, Hu H, Jiang K, Lin H, Ade H, Yan H. *Nat Commun*, 2014, 5: 5293
37 Long X, Ding Z, Dou C, Zhang J, Liu J, Wang L. *Adv Mater*, 2016, 28: 6504–6508
38 Jung JW, Jo JW, Chueh CC, Liu F, Jo WH, Russell TP, Jen AKY. *Adv Mater*, 2015, 27: 3310–3317
39 Fan Q, Su W, Guo X, Guo B, Li W, Zhang Y, Wang K, Zhang M, Li Y. *Adv Energy Mater*, 2016, 6: 1600430
40 Zhang S, Qin Y, Uddin MA, Jang B, Zhao W, Liu D, Woo HY, Hou J. *Macromolecules*, 2016, 49: 2993–3000
41 Kawashima K, Fukuhara T, Suda Y, Suzuki Y, Koganezawa T, Yoshida H, Ohkita H, Osaka I, Takimiya K. *J Am Chem Soc*, 2016, 138: 10265–10275
42 Scharber M , Mühlbacher D, Koppe M, Denk P, Waldauf C, Heeger A , Brabec C . *Adv Mater*, 2006, 18: 789–794
43 Zhang K, Huang F, Cao Y. *Acta Polym Sin*, 2017, 9: 1400
44 Zhang K, Hu Z, Sun C, Wu Z, Huang F, Cao Y. *Chem Mater*, 2017, 29: 141–148
45 Cowan SR, Roy A, Heeger AJ. *Phys Rev B*, 2010, 82: 245207